

DOI: 10.1002/cctc.201402469

Palladium Nanoparticles Supported on Magnesium Hydroxide Fluorides: A Selective Catalyst for Olefin Hydrogenation

Vaibhav R. Acham,^[a] Ankush V. Biradar,^[a] Mohan K. Dongare,^[a, b] Erhard Kemnitz,^{*[c]} and Shubhangi B. Umbarkar^{*[a]}

A one-pot synthesis of palladium nanoparticles supported on magnesium hydroxide fluoride has been performed with the fluorolytic sol–gel method. The prepared catalysts were characterized by using various physicochemical techniques. The sol–gel method led to high surface area ($> 135 \text{ m}^2 \text{ g}^{-1}$), mesoporous catalysts (pore volume = $0.19\text{--}0.23 \text{ cm}^3 \text{ g}^{-1}$, pore diameter = $3\text{--}5 \text{ nm}$) with uniformly dispersed palladium nanoparticles approximately 2 nm in diameter on the surface. The catalysts synthesized by using different concentrations of aqueous hydrofluoric acid exhibited changing surface and acidic properties. Very high dispersion of palladium on magnesium fluoride (47%) was obtained with $1 \text{ wt}\%$ palladium loading. The cata-

lysts were used for hydrogenation of various olefins in the presence of other organic functionalities at room temperature and atmospheric hydrogen pressure. Various substituted olefins were hydrogenated with almost 100% conversion and selectivity. The catalysts were recycled efficiently over five cycles without appreciable loss in catalytic activity. There was no palladium leaching under the reaction conditions, which was confirmed by inductively coupled plasma atomic emission spectroscopy analysis. Activation of olefin on the catalyst surface could not be observed by in situ FTIR studies, indicating facile activation of hydrogen on the palladium supported on magnesium hydroxide fluoride.

Introduction

A support plays a vital role in heterogeneous catalysis,^[1] hence a large number of supports have been explored for synthesis of efficient catalysts,^[2] which include carbon,^[3] silica-based structured supports,^[4] polymeric materials,^[5] and magnetic nanoparticles.^[6] The support not only adsorbs and desorbs reactants and products but also has a substantial influence on electron transfer,^[7] adsorption capacity,^[8] and the chemical and electronic structure of the active metal.^[9] Recently, many efforts have been devoted to the design and fabrication of supported metal catalysts by changing the crystal structure, morphology and crystallinity of supports.^[10] The metal–support interactions in catalysts depend on support characteristics such as surface area, crystal facets, and acidity or basicity, and catalyst crystal size.^[11]

Recently, one of us reported metal fluoride-based new type of nanoscopic, high-surface area, partly hydroxylated inorganic

fluorides with biacidic (Lewis and Brønsted) characteristics for fluorination and related processes,^[12] such as synthesis of (all-*rac*)- α -tocopherol,^[13] Suzuki coupling,^[14] synthesis of menthol,^[15] Friedel–Crafts reaction,^[16] syntheses of vitamins K₁ and K₂-chromanol,^[17] oxidation of ethylbenzene,^[18] dehydrohalogenation of 3-chloro-1,1,1,3,-tetrafluorobutane,^[19] C–H bond activation,^[20] and glycerol acetylation.^[21] Still, there is an enormous scope for the exploration of these supports in various organic transformations by taking advantage of their acidic and basic properties.

Palladium has been used extensively as a catalyst in many organic transformations, including the formation of C–C, C–O, and C–N bonds, oxidation, and hydrogenation.^[22] Hydrogenation of organic molecules is probably one of the most important chemical reactions for the synthesis of many compounds.^[23] These reactions can be catalyzed by homogeneous or heterogeneous catalysts, however, it is well recognized that heterogeneous catalysts are preferred from an industrial point of view,^[24] offering well-known benefits in terms of waste reduction and catalyst separation and recyclability.^[25] If present in the form of nanoparticles (NPs), the catalytic activity of palladium is known to increase considerably.^[26,27] This is closely linked to the development of stabilizing agents and supporting materials such as metal oxides,^[28] ionic liquids,^[29] polymers,^[30] dendrimers,^[31] and carbonaceous materials.^[32] Palladium-based catalysts including palladium supported, for example, on carbon are widely used to hydrogenate organic functionalities, such as alkyne, alkene, azide, nitro, benzyl ether,

[a] V. R. Acham, A. V. Biradar, M. K. Dongare, S. B. Umbarkar
Catalysis Division, CSIR-National Chemical Laboratory
Dr. Homi Bhabha Road, Pune—41108 (India)
E-mail: sb.umbarkar@ncl.res.in

[b] M. K. Dongare
Mojj Engineering Systems Ltd
15-81/B, MIDC, Bhosari, Pune—411026 (India)

[c] E. Kemnitz
Institute of Chemistry
Humboldt University, Berlin
Brook-Taylor-Straße 2, 12489 Berlin (Germany)
E-mail: erhard.kemnitz@chemie.hu-berlin.de

 Supporting information for this article is available on the WWW under <http://dx.doi.org/10.1002/cctc.201402469>.

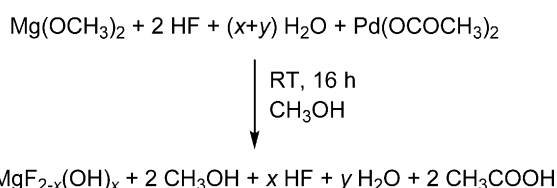
benzyl ester, aromatic halide, aromatic ketone, *N*-benzyloxycarbonyl, and epoxide groups in organic syntheses.^[33]

Although significant progress has been achieved in improving catalytic activity, selectivity, and substrate scope, drastic reaction conditions such as high pressure and high temperature required for hydrogenation using palladium catalysts lead to agglomeration of palladium, which causes catalyst deactivation. Palladium leaching is another severe problem faced in many industrial processes and needs to be addressed.^[34] The replacement of expensive high-energy processes by inexpensive, low-energy and environmentally benign processes is a desirable goal in hydrogenation. Hydrogenation under ambient temperature and pressure is ideal for industry. In continuation of our efforts in exploring metal fluorides as catalysts or catalyst supports, we have prepared palladium supported on nanoscopic magnesium fluoride by a one-pot fluorolytic sol-gel route and used it in the selective hydrogenation of various olefins under ambient reaction conditions, the results of which are reported herein.

Results and Discussions

Catalyst synthesis

Palladium supported on magnesium fluoride was synthesized by the fluorolytic sol-gel route with magnesium methoxide as precursor (Scheme 1). For fluorolysis, in situ-prepared magnesi-



Scheme 1. One-pot sol-gel synthesis of different Pd-MgF_{2-x}(OH)_x phases.

um methoxide was reacted with different concentrations of hydrofluoric acid (HFA), 100% (alcoholic) and 71 and 40% (aqueous), to obtain magnesium fluorides and hydroxide fluorides. During fluorolysis, two competitive reactions—hydrolysis and fluorolysis (fluorination)—of metal methoxide took place. Depending on the concentration of HFA, the extent of fluorination and hydrolysis varied to give Pd-MgF_{2-x}(OH)_x.^[35] Although the fluorination was dominant, the hydrolysis of magnesium alkoxide became competitive with increasing water content in the medium, resulting in a continuous change in the degree of fluorination.^[36] By adding the palladium precursor during sol-gel synthesis of MgF_{2-x}(OH)_x, the one-pot synthesis of palladium supported on magnesium hydroxide fluoride was achieved. According to the concentration of HFA used [100% (alcoholic) or 71 or 40% (aqueous)] for the synthesis, the catalysts were denoted as Pd-MgF₂-100, Pd-MgF₂-71 and Pd-MgF₂-40 respectively. The non-aqueous sol-gel route resulted in the formation of clear sols and transparent gels, whereas the aqueous route always resulted in opaque gels.^[36]

Catalyst characterization

All catalysts were reduced by bubbling hydrogen gas through a suspension of catalyst in methanol before structural analysis and characterization by nitrogen physisorption measurements, FTIR, UV/Vis, TEM, powder X-ray diffraction (XRD), X-ray photoelectron spectroscopy (XPS), and elemental analyses.

The XRD patterns of all catalysts (see Figure 1) showed the typical diffraction patterns of magnesium fluoride, which were

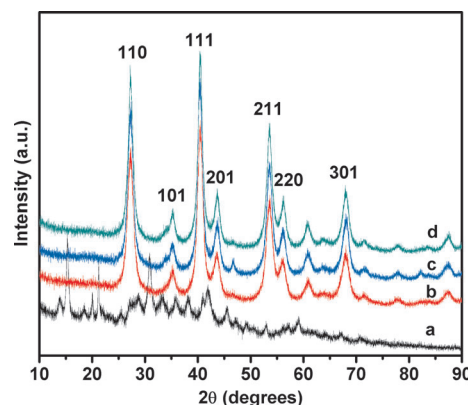


Figure 1. XRD patterns of a) Pd-MgO b) Pd-MgF₂-40 c) Pd-MgF₂-71 d) Pd-MgF₂-100.

also characteristic of the Mg(OH)_{2-x}F_x phases. The XRD patterns of the fluorinated catalysts showed a broadening in peak pattern compared to the pure rutile structure type with small crystallite size. There was no significant difference observed between the XRD patterns of Pd-MgF₂-40, Pd-MgF₂-71, and Pd-MgF₂-100 (Figure 1 b–d, respectively), which indicated that the MgF₂-structure of Pd-MgF_{2-x}(OH)_x as formed tolerated hydroxyl groups and the crystal phase did not change with the amount of water used during the synthesis. Thus, the crystal structure formation was not affected by the F/OH ratio. Moreover, this was clear evidence that the competitive hydrolysis reaction by water was suppressed in the presence of the significantly stronger reactant HFA. Hence, fluorolysis strongly dominated over hydrolysis. The XRD pattern of Pd-MgO prepared for comparison also showed broad peaks, confirming the nanoscopic nature of this catalyst as well (Figure 1 a). In line with former investigations, the XRD patterns showed no deviation from the MgF₂-structure although magnesium hydroxide fluoride phases (MgF_{2-x}(OH)_x) with low OH content were formed.

The prepared catalysts were characterized by FTIR spectroscopy (see the Supporting Information, Figure S1). Owing to the octahedral coordination of magnesium by fluorine and O(H), all catalysts exhibited the expected OH symmetry for an ordered structure with two infrared active modes. In fluorinated catalysts, typically Mg–F and Mg–O stretches were observed at 460 and 552 cm⁻¹, respectively. The bands present at 3713 and 3432 cm⁻¹ indicated the presence of isolated and bridging hydroxyl groups or adsorbed water molecules, respectively. The bands in the range of 2750–3200 and 1050–1150 cm⁻¹ were assigned to C–H and C–O stretching vibrations, respec-

Catalyst	Physisorption ^[a]			Acidity ^[b]		Chemisorption ^[c]			
	Surface area [m ² g ⁻¹]	Mean pore diameter [nm]	Pore volume [cm ³ g ⁻¹]	NH ₃ adsorbed [mmol g ⁻¹]	Peak max. [°C]	H ₂ adsorbed [mmol g ⁻¹] × 10 ⁻⁵	Pd dispersion [%]	Metal surface area [m ² g ⁻¹]	Mean particle diameter [nm]
Pd–MgF ₂ -100	136	5.0	0.21	0.328	240	2.22	47.29	2.10	2.36
Pd–MgF ₂ -71	145	4.0	0.19	0.208	210	2.14	45.71	2.03	2.40
Pd–MgF ₂ -40	148	3.3	0.23	0.173	150	1.58	33.62	1.49	3.33
Pd–MgO	255	4.9	0.21	–	–	–	–	–	–

Determined by [a] BET surface area, [b] NH₃-TPD, or [c] H₂ temperature-programmed reduction analysis.

tively. In case of Pd–MgO, very weak vibrations were observed in the range of 3000–2750, 1463, and 1101 cm⁻¹, indicating the presence of few methoxy functionalities and carbonate groups in the catalyst. The band between 1650–1600 cm⁻¹ corresponding to O–H bending vibrations was observed as a result of adsorbed water or surface O–H groups. The FTIR spectrum of Pd–MgO showed peaks corresponding to magnesium carbonate at 1463, 2790–2925, 3379 and 3697 cm⁻¹, which matched well with literature reports.^[37]

Nitrogen adsorption investigations were performed to study the effect of fluorination on alteration of surface area, pore diameter, and volume. The adsorption isotherms (see Figure S2) and resulting data are summarized in Table 1. All catalysts showed a very high surface area of around 136 m²g⁻¹ compared to 40–45 m²g⁻¹ for MgF₂ or MgO prepared by conventional methods.^[38] All isotherms showed type IV character typical of mesoporous materials with a H1-type hysteresis loop and porous texture. The BET surface area of all catalysts showed a decrease in the order Pd–MgO (255 m²g⁻¹) > Pd–MgF₂-40 (148 m²g⁻¹) > Pd–MgF₂-71 (145 m²g⁻¹) > Pd–MgF₂-100 (136 m²g⁻¹). In Pd–Mg(OH)_{2-x}F_x, the surface area changed with variation of the concentration of aqueous HFA used for fluorination, which affected the degrees of fluorination and hydrolysis. The fluorinated catalysts showed a mesoporous nature with a decreasing trend in pore size on decreasing the concentration of HFA used for synthesis. The pore diameter of Pd–MgO was in the mesoporous range. In total pore volume studies, no trend was observed. The pore volume for all catalysts was found to be in the range of 0.19–0.23 cm³g⁻¹.

The total acidity and the strength of acidic sites on the surface of the catalysts were determined by NH₃ temperature-programmed desorption (TPD) analysis and the results presented in Table 1 and Figure S3. The extent of fluorination against hydrolysis was found to depend on the concentration of HFA used and decreased expectedly with increase in the water content of HFA. NH₃-TPD results indicated a decrease in total acidity of the catalysts in the order Pd–MgF₂-100 (0.328 mmol g⁻¹) > Pd–MgF₂-71 (0.208 mmol g⁻¹) > Pd–MgF₂-40 (0.173 mmol g⁻¹). The peak maximum was observed for Pd–MgF₂-100 at 240 °C, which decreased to 210 °C for Pd–MgF₂-71 and further to 120 °C only for Pd–MgF₂-40. This decrease in desorption temperature was correlated with acid strength, which decreased from Pd–MgF₂-100 to Pd–MgF₂-40. The peak maximum for Pd–MgF₂-40 (120 °C) was very low, thus indicating very weak acidic sites. As no desorption peak below 150 °C

was observed for the other two samples (Pd–MgF₂-100 and Pd–MgF₂-71) analyzed under identical conditions, assignment to physisorbed NH₃ was not reasonable; this rather evidenced very weak acidic sites on Pd–MgF₂-40.

The type of acidity present on the catalyst surface was studied by FTIR–photoacoustic spectroscopy studies of adsorbed pyridine (pK_a = 5.25; see Figure 2). The spectra of Pd–MgF₂-100, Pd–MgF₂-71, and Pd–MgF₂-40 indicate the presence of intense bands at 1445, 1490, and 1576 cm⁻¹, which are characteristic of strong Lewis acid sites. The strength of Lewis acidity decreased in the order Pd–MgF₂-100 > Pd–MgF₂-71 > Pd–MgF₂-40, which was in agreement with NH₃-TPD results. The origin of Lewis acidity on the surface of the catalyst can be rational-

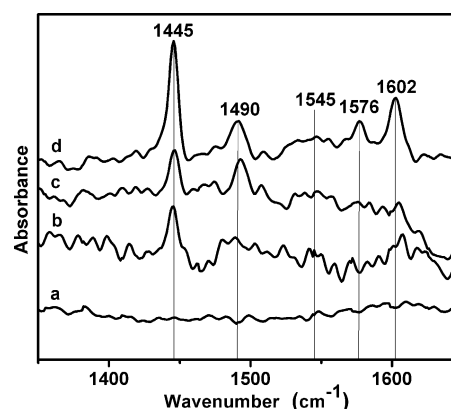


Figure 2. Diffuse-reflectance FTIR adsorbed pyridine spectra of a) Pd–MgO, b) Pd–MgF₂-40, c) Pd–MgF₂-71, and d) Pd–MgF₂-100.

ized by the presence of four or five-coordinated Mg surface sites (Figure 3a) and is attributed to the presence of more electron-withdrawing fluorine atoms attached to five-coordinated Mg sites as reported previously.^[39] The peak at 1545 cm⁻¹ showed higher intensity in Pd–MgF₂-40 than the other fluorinated catalysts. The Brønsted acidity may have been generated as a result of the presence of Mg, which was coordinated by fluorine and hydroxyl groups. In such cases, owing to the highly electronegative fluorine atoms, the bonded electrons migrated towards fluorine thus causing a weakening of the O–H bond. The weak O–H bond could lose a proton and behaved as a Brønsted acid (Figure 3b). A steady decrease in the Lewis and increase in Brønsted acidity was observed for Pd–MgF₂-71 and Pd–MgF₂-40. As expected,

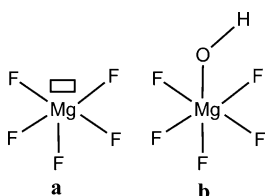


Figure 3. a) Generation of Lewis acidity owing to the presence of five-coordinated Mg-sites in MgF_2 . b) Generation of Brønsted acidity of an OH group present in MgF_2 .

Pd-MgO did not show any surface acidity. Thus, the Lewis acidity of the Pd-MgF_2 -based catalysts decreased in the order $\text{Pd-MgF}_2\text{-100} > \text{Pd-MgF}_2\text{-71} > \text{Pd-MgF}_2\text{-40} > \text{Pd-MgO}$. This order corresponded well to the trend first observed for pure magnesium hydroxide fluorides.^[40] It is commonly accepted that bonds in Mg-OH fragments are polarized in such a way that the Mg-O bond is significantly more polar than the O-H bond in pure Mg(OH)_2 , thus resulting in

cleavage of the Mg-O bond under the action of a solvent, such as water. Consequently, MgO in water and Mg(OH)_2 are basic in nature. On the other hand, in chemically pure MgF_2 there are no OH groups, thus just Lewis acidity might be expected provided that coordinative unsaturated Mg surface sites are present.

This condition is fulfilled in nanoscopic MgF_2 based on high-surface area material providing a high degree of structural distortion, though it is very limited in case of crystalline MgF_2 . If, however, a very small number of hydroxyl groups are introduced into MgF_2 , the situation is different to that described above. As proven by magic-angle spinning ^{19}F NMR spectroscopy, the $\text{Pd-MgF}_2\text{-100}$, $\text{Pd-MgF}_2\text{-71}$, and $\text{Pd-MgF}_2\text{-40}$ samples contain highly distorted $\text{MgF}_{6-x}(\text{OH})_x$ octahedral building blocks.^[41] Notably, the stoichiometric number x increases with decrease in concentration of HFA used in the synthesis procedure. Thus, different to the situation of an Mg-O-H unit in MgO or Mg(OH)_2 , in the Pd-MgF_2 -samples, the OH groups are located in a fluorine-rich structural environment. Owing to the strong electron-withdrawing nature of fluoride, the positive charge on the Mg^{2+} ion is further strengthened, thus inducing an electron density shift, and hence a further polarization of the O-H bond. This strong polarization of the O-H bond in a fluorine-rich structural environment alters the nature of the catalyst from basic to acidic, as discussed comprehensively for the series of pure magnesium hydroxide fluorides.^[41]

The Pd dispersion was determined by H_2 chemisorption studies and results are given in Table 1. According to literature reports, PdO on heterogeneous metal fluoride supports is reduced at low temperatures.^[42] Hence the H_2 consumption profiles of the present samples were recorded from 50 to 300 °C. The amount of H_2 adsorbed on Pd-supported catalysts varied from 2.22×10^{-5} to 1.58×10^{-5} mmol g^{-1} . Although there was no significant difference in the surface area of the supports, the metal surface area and percentage palladium dispersion showed a decreasing trend in the order $\text{Pd-MgF}_2\text{-100} > \text{Pd-MgF}_2\text{-71} > \text{Pd-MgF}_2\text{-40}$. $\text{Pd-MgF}_2\text{-100}$ and $\text{Pd-MgF}_2\text{-71}$ exhibited approximately 47 and 46% Pd dispersion. This Pd dispersion was extremely high compared to Pd dispersed on commercial carbon of very high surface area ($1400 \text{ m}^2 \text{ g}^{-1}$), which was reported to give only 30% dispersion for 1% Pd loading.^[43] The higher Pd dispersion ($\approx 47\%$) on the MgF_2 catalyst with $136 \text{ m}^2 \text{ g}^{-1}$ surface area compared to very high surface

area carbon may be attributed to the in situ sol-gel synthesis approach leading to a very high dispersion and decrease in the particle size of Pd. The Pd particle size determined from H_2 chemisorption studies was found to be in the range of 2.4–3.3 nm.

XPS was used to determine the effect of the support on the oxidation state of Pd of the synthesized samples. The $\text{Pd-MgF}_2\text{-100}$ catalyst was compared with Pd-MgO and commercial 5% Pd/C (Sigma-Aldrich), as shown in Figure 4. The binding energies (BE) of Pd in Pd-MgO and Pd/C were identical (336.9 eV), indicating that Pd was in the zero oxidation state, whereas for $\text{Pd-MgF}_2\text{-100}$, a considerable shift in BE values from 336.9 to 338.9 eV was observed. The BE value of 338.9 eV corresponds to the presence of Pd^{2+} species on the surface, the origin of which may be the palladium acetate used as Pd

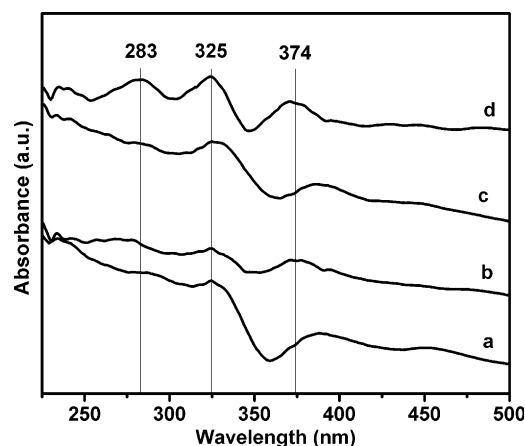


Figure 4. XPS spectra of a) Pd/C (commercial), b) $\text{Pd-MgF}_2\text{-100}$, and c) Pd-MgO .

precursor. Commercial 5% Pd-C showed two peaks at 336.9 and 342.2 eV corresponding to Pd^0 and PdO, respectively. The presence of Pd^{2+} species indicated the presence of oxidized Pd in the form of PdO. There was no peak corresponding to PdO observed in the XPS spectra of $\text{Pd-MgF}_2\text{-100}$ and Pd-MgO , indicating the absence of PdO on these surfaces.

The considerable shift in the binding energy of Pd^{2+} (338.9 eV) in $\text{Pd-MgF}_2\text{-100}$ from Pd^{2+} (338.6 eV) in the precursor palladium acetate^[44] indicates a significant electron-withdrawing effect caused by MgF_2 , suggesting a strong metal-support interaction. Clearly, the fluoride-rich structural environment in the highly distorted MgF_2 -lattice withdraws electron density from the Pd, inducing partial Lewis acidity at the precious metal. Hence, partial positive charge on Pd in case of $\text{Pd-MgF}_2\text{-100}$ contributes additionally to the acidity of the catalyst, which has also been confirmed by $\text{NH}_3\text{-TPD}$ studies. It is known that Pd^0 is the active state of Pd for hydrogenation, however, partially positive charge on Pd is reported to be even more active for hydrogenation.^[45]

To study the interaction of Pd with the MgF_2 support, UV/Vis spectra of the prereduced catalysts were recorded (Figure 5). The band at 283 nm matched well with $[\text{Pd}]^{2-}$ species previously reported.^[46] The bands around 325 nm were assignable

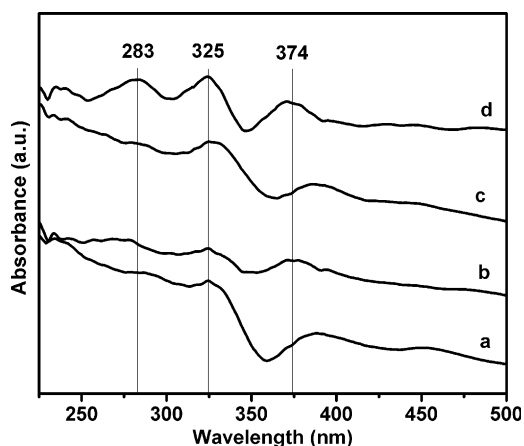


Figure 5. UV/Vis spectra of a) Pd–MgF₂-100, b) Pd–MgF₂-71, c) Pd–MgF₂-40, and d) Pd–MgO.

to the d–d transition of Pd species.^[47] The bands at 374 nm may correspond to a charge-transfer band in the Pd species in a strongly electronegative environment. With increasing ligand electronegativity, the partial positive charge on the metal increases resulting in a bathochromic shift in the UV bands. The bands around 283, 325, and 374 nm of Pd–MgF_{2-x}OH_x are less intense than those of Pd–MgO. These results clearly confirm a strong metal–support interaction of Pd with magnesium fluorides and/or hydroxide fluorides. Thus, these results are in line with results obtained by XPS analysis.

The change in the morphology of the catalysts with the HFA concentration used in the syntheses was studied by SEM (see Figure S4). The results clearly indicate the effect of dilution of HFA on the textural properties of the final catalysts. HFA concentration not only affected the crystallite size but also the surface morphology. Catalyst particle size decreased with HFA concentration. Pd–MgF₂-100 showed very large crystals, whereas Pd–MgF₂-71, Pd–MgF₂-40, and Pd–MgO showed sheet-like structures of variable size with a small number of very small crystallites. Furthermore, the surface compositions of all catalysts were determined by energy-dispersive X-ray (EDX) analyses (see Table 2), which showed the presence of almost 1 wt% Pd on the surface, indicating uniform dispersion and availability of all loaded Pd on the surface for the reaction.

The particle size of magnesium hydroxide fluoride and palladium nanoparticles was estimated by using high-resolution TEM analysis (Figure S5). Previously, we showed that MgF₂ prepared by the fluorolytic sol–gel route led to the formation of nanoscopic MgF₂ with particle sizes in the range of 6–10 nm.^[48] The representative micrographs of Pd nanoparticles are shown in Figure 6. The particle size distribution studied by TEM clearly showed the majority of particles are approximately 5 nm in diameter, though the particle size distribution spreads up to 20 nm. The palladium particles were found to be in the (111) plane as identified by measuring the *d* spacing (*d*₁₁₁ =

Table 2. Elemental analysis of catalysts by EDX.				
Catalyst	Elemental composition			
	Pd	Mg	F	O
Pd–MgF ₂ -100	0.99	39.57	55.70	3.74
Pd–MgF ₂ -71	1.20	39.34	54.26	5.21
Pd–MgF ₂ -40	0.93	39.02	51.20	8.85
Pd–MgO	0.89	58.20	0.0	40.91

0.223 nm). The *d* spacing for MgF₂ also confirmed the presence of (110) (*d*₁₁₀ = 0.326 nm) and (111) (*d*₁₁₁ = 0.222 nm) planes (Figure 6a–c). In case of the Pd–MgO catalyst, *d* spacing confirmed the formation of the (111) plane of Pd (*d*₁₁₁ = 0.223 nm) and MgO (*d*₁₁₁ = 0.243 nm), which indicated a semicrystalline nature of MgO. The formation of small Pd particles was attributed to the fluorolytic sol–gel preparation, which enabled very high dispersion and small particle size. There was no appreciable difference observed in the particle size distribution of all catalysts.

The catalysts showed very high metal dispersion compared to literature reports.^[43] The high metal dispersion on relatively low surface area catalysts is due to the formation of palladium metal nanosheets on the surface of sol–gel-synthesized magnesium fluorides. With fluorinated catalysts, palladium showed nanosheet-like structures, whereas spherical nanoparticle formation was observed with magnesium oxides.

The catalytic activity of the palladium-supported magnesium hydroxide fluoride was evaluated for olefin hydrogenation, initially with styrene as model substrate (Scheme 2). The hydrogenation was performed at room temperature and atmospheric

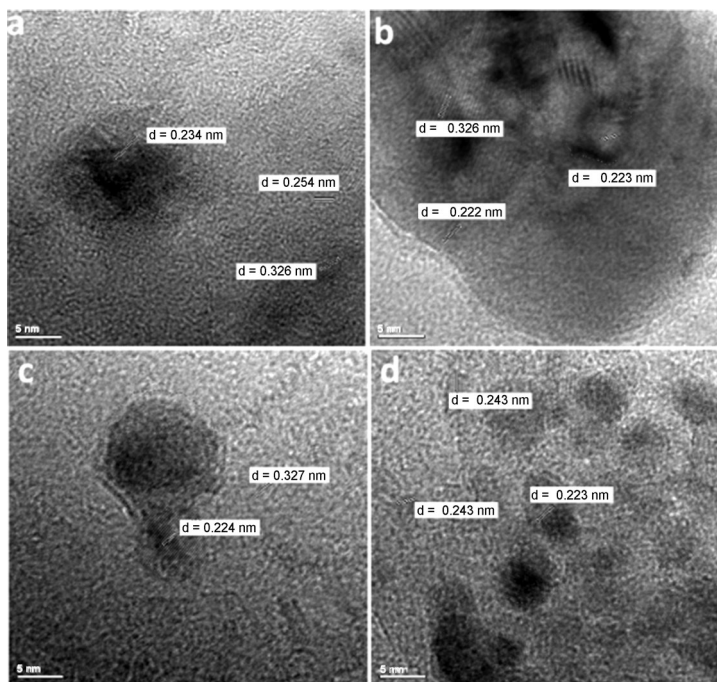
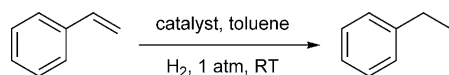


Figure 6. TEM images of catalysts a) Pd–MgF₂-100, b) Pd–MgF₂-71, c) Pd–MgF₂-40, and d) Pd–MgO. Scale bars = 5 nm.

ic pressure by bubbling hydrogen gas through the reaction mixture. On performing reactions under identical conditions for comparison without catalyst, with Pd–MgO catalyst, and with commercial 5 wt% Pd/C catalyst, very poor styrene conversions of <1, 7, and 4%, respectively, were obtained (Table 3, entries 1–3). On performing the reaction with Pd–MgF₂-40 catalyst, 44% styrene conversion was obtained after



Scheme 2. Hydrogenation of styrene.

3 h (entry 4), which was increased to 71% with Pd–MgF₂-71 (entry 5) and further increased to 100% with Pd–MgF₂-100 under identical reaction conditions (entry 6). All reactions were selective towards the catalytic hydrogenation of olefinic double bonds. Aromatic ring hydrogenation was not observed in any of the reactions. The catalyst Pd–MgF₂-100 showed 100% conversion with a maximum rate constant of $11.9 \times 10^{-3} \text{ s}^{-1}$.

Entry	Catalyst	Conv. ^[b] [%]	Sel. ^[b] [%]	Rate constant ^[c] [s ⁻¹]
1	–	< 1	100	–
2	5% Pd/C	4	100	–
3	Pd–MgO	7	100	–
4	Pd–MgF ₂ -40	44	100	2.12×10^{-3}
5	Pd–MgF ₂ -71	71	100	10.60×10^{-3}
6	Pd–MgF ₂ -100	≈ 100	100	11.93×10^{-3}

[a] Reaction conditions: 1.0 mmol styrene, 0.01 g catalyst (10 or 0.1 wt% Pd with respect to styrene), 6.0 mL toluene solvent, bubbling H₂, RT (27 °C), *t* = 3 h. [b] Determined based on GC analysis, [c] Determined by assuming a reaction that follows 1st order kinetics over the first 10 min.

The effect of catalyst loading on styrene hydrogenation was studied by using the Pd–MgF₂-100 catalyst (Figure S6). On increasing the catalyst loading with respect to styrene gradually from 2 to 20 wt%, the conversion after 1 h increased gradually from 6 to 65%. The increase in catalyst loading caused an increase in conversion without affecting selectivity. However, to balance between catalytic loading and catalytic activity, 10 wt% catalyst loading was used for further reactions.

To study the wider applicability of the catalyst for olefin hydrogenation, various substrates were studied (see Table 4). In the case of styrene, the reaction was completed within 3 h with 100% selectivity for ethylbenzene (Table 4, entry 1). If cyclohexene, cyclooctene, and *n*-hexene were hydrogenated under identical conditions, the time required for complete conversion to the desired hydrogenated products was longer compared to hydrogenation of styrene, indicating a lower reactivity of these substrates (Table 4, entries 2–4). To expand the hydrogenation study to disubstituted olefins, indene and α -methyl-

styrene were screened, however lower activity compared to styrene was obtained (15 and 8% conversion, respectively, after 1 h). The lower activity could have owed to the higher order of substitution of these olefins (entries 5–6). To study the hydrogenation of olefins in presence of other reducible functional groups, 2-butenal was hydrogenated with 100% selectivity for olefin hydrogenation without reduction of the ketone moiety (entry 7). In case of 2-alkenol, olefinic hydrogenation was competitive with isomerization reaction.^[47] To study the selectivity pattern in such substrates, 3-phenylpropenol was selected as the representative substrate, which on reaction showed 100% conversion with >99% selectivity for 2-phenylpropanol (entry 8). On hydrogenation of olefins with carboxylic

Table 4. Catalytic hydrogenation of various olefins using Pd–MgF₂-100.^[a]

Entry	Substrate	<i>t</i> [h]	Conv. [%]	Sel. [%]	Normalized TOF ^[b] [h ⁻¹]
1		1	29	100	634
		3	≈ 100	100	
2		1	7	100	197
		12	≈ 100	100	
3		1	13	100	301
		8	≈ 100	100	
4		1	9	100	243
		10	≈ 100	100	
5		1	15	100	266
		6	≈ 100	100	
6		1	8	100	150
		12	≈ 100	100	
7		1	13	99	411
		9	≈ 100	99	
8		1	6	99	108
		12	≈ 100	99	
9		1	17	99	230
		6	≈ 100	99	
10		1	24	99	369
		5	100	99	
11		1	16	99	178
		6	65	99	
12 ^[c]		1	18	99	232
		6	89	99	
13 ^[c]		1	15	99	185
		6	66	99	
14 ^[c]		1	18	99	302
		6	95	99	
15 ^[c]		1	12	99	252
		12	78	99	

[a] Reaction conditions: 1.0 mmol alkenes, Pd–MgF₂-100 catalyst (10 wt% with respect to substrate, 0.1 wt% of Pd), 6.0 mL toluene solvent, H₂ bubbling, RT (27 °C). [b] Turnover frequencies related to the active sites of Pd, as determined by hydrogen adsorption–desorption measurements. [c] *T* = 80 °C.

group functionality such as methyl acrylate and acrylic acid, 100% conversions with almost complete selectivity to methyl propanoate and propanoic acid, respectively, were obtained (entries 9–10). The high conversions indicated stability of the catalysts in the presence of carboxylic and electron-withdrawing groups, which activated the olefinic C=C for catalytic hydrogenation. The effect of bulkier groups and electron-withdrawing reducible carbonyl groups was studied by using benzalacetophenone as substrate. The conversion decreased to 65% without affecting much the selectivity to 1,5-diphenylpentanone. This lowered activity indicated a negative effect of steric hindrance owing to the presence of phenyl rings (entry 11). The geometrical isomers, *cis* and *trans* stilbene were hydrogenated. The hydrogenation needed a slightly elevated temperature (80 °C) owing to higher steric hindrance of the bulkier phenyl group. *trans*-Stilbene showed lower activity than the *cis* isomer. This may have owed to the higher relative stability of the *trans* isomer than the *cis* isomer (entries 12–13). Furthermore, the effect of the substituent on the phenyl ring of styrene was examined by catalytic hydrogenation of 4-vinylanisole. The reaction showed 95% conversion with 99% selectivity for olefin hydrogenation (entry 14). If 2-vinylpyridine was used as substrate to study olefinic hydrogenation in a heterocyclic system, 78% conversion with 99% selectivity was achieved at 80 °C after 12 h (entry 15). This substrate screening study showed sterically hindered olefins to be less reactive for catalytic hydrogenation. The catalyst showed selectivity for olefinic hydrogenation in the presence of other reducible functional groups such as carbonyl and carboxylic groups. In addition, sterically hindered olefins could be hydrogenated at elevated reaction temperatures.

The recyclability of the catalyst was tested by using styrene hydrogenation as the model reaction under the conditions given in Table 3. After completion of each reaction the catalyst was separated, washed, dried, and reused for the next run, the results of which are summarized in Figure S7. The catalyst could be recycled very efficiently over five cycles without appreciable decrease in styrene conversion. Possible Pd leaching was investigated by separating the catalyst from the reaction mixture by filtration after 1.5 h (57% styrene conversion) and continuing the reaction (in the filtrate) without the catalyst. However, even after continuing the reaction for an additional 3 h, there was no increase in styrene conversion (Figure S8), which strongly evidenced the absence of Pd leaching from the catalyst. Additionally, Pd leaching was also tested by using inductively coupled plasma atomic emission spectroscopy, which showed no indication of Pd leaching into the reaction medium (at a Pd metal detection limit of 5 ppm). Therefore, Pd–MgF₂-100 acted as true heterogeneous catalytic system without leaching. The TEM image of a recycled Pd–MgF₂-100 catalyst (after five cycles) revealed only a slight agglomeration of Pd on the catalyst surface (Figure S9). In the fresh catalyst (Figure 6), formation of Pd sheets was observed whereas in the recycled catalyst, Pd particles approximately 6 nm in diameter were observed indicating partial agglomeration. However, there was no decrease in the catalytic activity in successive

cycles indicating that even these Pd particles on MgF₂ were equally active for hydrogenation.

Kantam et al. recently reported the use of palladium supported on lanthanum-modified magnesium oxide nanoparticles, Pd/La-MgO, as an efficient catalyst for the chemoselective hydrogenation of olefinic double bonds at room temperature and atmospheric pressure. However, 10 wt% Pd loading had been used for this transformation. As the surface area of the support was low ($\approx 35 \text{ m}^2 \text{ g}^{-1}$) the palladium particles obtained were larger, for example, in the range of 28–32 nm.^[49] In another report, Asefa et al. used Pd encapsulated in poly(amido amine) dendrimers supported on silica microspheres. The reported activity was very high for room temperature hydrogenation of olefins, nitro aromatics, and carbonyl compounds even with very low palladium loading and very high turnover frequencies were reported ($24\,000 \text{ h}^{-1}$). However, the hydrogenation was effective only at higher pressures and the catalyst preparation involved multistep preparation.^[50]

The results obtained in the present study are superior to previous reports, indicating the positive effect of magnesium hydroxide fluorides as support on the catalytic activity of palladium nanoparticles. The results obtained for Pd–MgF₂-100 can be correlated with the acidity of the surface of the catalyst, size of the Pd nanoparticles, hydrogen adsorption capacity of the catalyst, partial positive charge on the Pd sites, and strong metal–support interaction. On comparison of the Pd–MgF₂-100 catalyst with other catalysts, it showed distinct characteristics of high specific surface acidity equivalent to 0.328 mmol of NH₃ and high hydrogen adsorption capacity equivalent to $2.22 \times 10^{-5} \text{ mmol g}^{-1}$ of catalyst.

Owing to the high hydrogen adsorption capacity of the catalyst, it exhibited high metal dispersion of up to 47% as a result of smaller metal particle formation and higher metal surface area. Also, XPS studies showed the presence of electron-deficient Pd with partial positive charge, which activated olefins after adsorption and helped in catalytic hydrogenation compared to other catalysts such as Pd on charcoal.

In situ FTIR study and reaction mechanism

To study the effect of support on palladium-catalyzed hydrogenation reactions, in situ FTIR studies were performed by passing hydrogen and styrene over the catalyst surface in diffused-reflectance mode and monitoring the formation of species on the catalyst surface (Figure 7). Initially, only styrene was passed across the catalyst surface at room temperature with a flow of nitrogen gas to study if activation of styrene took place (Figure 7c). However, the activation of styrene could not be observed on the catalyst surface as no significant shifts in the olefinic C=C band (1600 cm^{-1}) and C–H stretching frequency (in the range $2873\text{--}3085 \text{ cm}^{-1}$) were observed relative to those of styrene from the FTIR database (Figure 7a). This indicated that only physisorption of styrene on the catalyst surface occurred. Then, hydrogen gas was passed over the catalyst surface already saturated by physisorbed styrene and instantaneous formation of ethyl benzene was observed on the catalyst surface with a corresponding decrease in intensity of styrene peaks

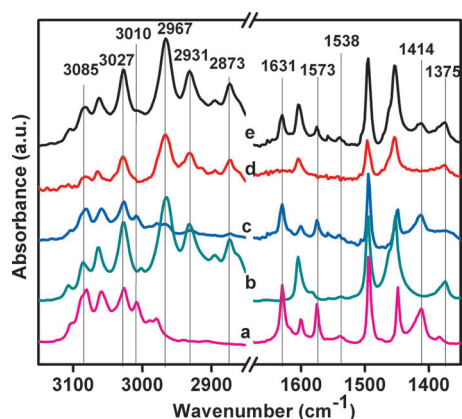


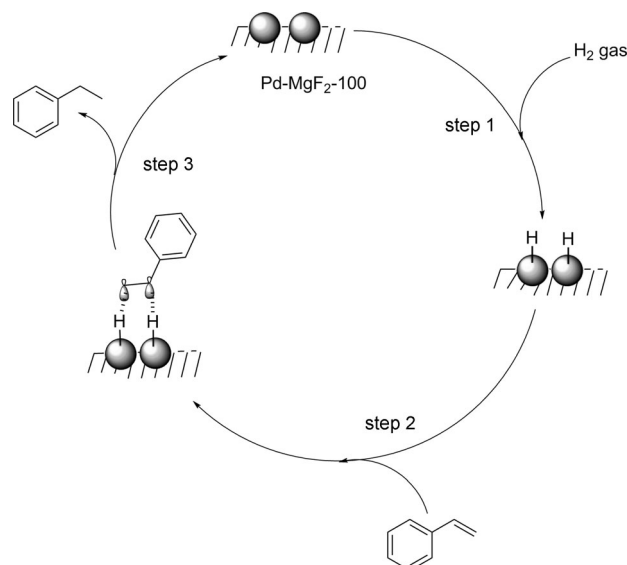
Figure 7. In situ FTIR difference spectra for study of the hydrogenation reaction on catalyst Pd–MgF₂-100: a) styrene, b) ethylbenzene, c) catalyst + styrene in nitrogen flow, d) catalyst + styrene in nitrogen + hydrogen flow, and e) catalyst + styrene in hydrogen flow.

(Figure 7d). If styrene and hydrogen were passed together over the catalyst surface (Figure 7e), instantaneous ethyl benzene formation was observed along with very low intense peaks for styrene, which clearly indicated a facile activation of hydrogen on palladium under ambient reaction conditions and further reaction with physisorbed styrene on the catalyst surface. Previously, Wojciechowska et al. have used Pt–MgF₂ for the chemoselective hydrogenation of chloronitrobenzene. Pt–MgF₂ was prepared by precipitation with magnesium carbonate as the magnesium precursor and platinum loading by the conventional impregnation method.^[51] Chemoselective hydrogenation of the nitro group resulted from the activation of nitrobenzene on Pt–MgF₂ and on MgF₂, which was proven by in situ FTIR studies.^[51] Although in the present case, sol–gel synthesized Pd–MgF₂ was used, no activation of the substrate (olefin) on the catalyst surface could be detected, rather facile hydrogenation of olefin under ambient reaction conditions was observed.

Based on the FTIR studies, the proposed mechanism for hydrogenation of styrene on Pd–MgF₂-100 is shown in Scheme 3. As indicated by FTIR results, initial activation of hydrogen takes place on palladium (step 1) followed by the interaction of styrene with activated hydrogen (step 2) forming ethyl benzene that liberates to regenerate the catalyst (step 3).

Conclusions

Palladium supported on nanoscopic magnesium fluoride by facile one-pot fluorolytic sol–gel route yielded very efficient catalysts for chemoselective hydrogenation of olefins in the presence of other functionalities under ambient reaction conditions and bubbling of hydrogen gas. The catalyst was recycled efficiently up to five cycles without appreciable loss in catalytic activity. There was no palladium leaching during the reaction as confirmed by inductively coupled plasma atomic emission spectroscopy analysis. Activation of styrene was not observed on the catalyst surface by in situ FTIR studies, which



Scheme 3. Proposed reaction mechanism for hydrogenation of styrene by using the Pd–MgF₂-100 catalyst.

indicated that a facile activation of hydrogen on palladium gave very high activity under ambient conditions.

Experimental Section

Materials

All chemicals were procured from Aldrich and used as received. HFA with various concentrations [100% (alcoholic), 71 and 40% (aqueous)], and solvents were purchased from Merck and used as obtained. Solvents were freshly dried before use according to the literature procedure.^[52]

Catalyst synthesis

CAUTION: HFA is a highly toxic and irritant compound causing severe burns if it comes in contact with the skin! It is advised to use full safety wear.

Catalyst were prepared under an argon atmosphere by using the standard Schlenk technique. The series of palladium supported on magnesium hydroxide fluoride catalysts was prepared from metallic magnesium by using the sol–gel method as follows: In a 250 mL round-bottom flask, metallic magnesium (1.56 g, 64 mmol) was dissolved in dry methanol (100 mL) at RT for 16 h to form the methanolic solution of magnesium methoxide. To this magnesium methoxide solution, a stoichiometric amount (2 equiv.) of HFA (130 mmol) of different concentrations [100% (alcoholic), 71 and 40% (aqueous)] was added followed by addition of a methanolic solution of palladium acetate (0.845 g, 3.77 mmol) with 1 wt% palladium loading. The mixture was allowed to react to form a highly viscous opaque gray-colored gel. The gel was aged for 12 h, then dried under vacuum initially at RT for 3 h then at 60 °C for 3 h until the methanol was completely removed. The solid product was dried further at 250 °C for 5 h. Based on the concentration of HFA used for synthesis, the catalysts were referred as Pd–MgF₂-40, Pd–MgF₂-71, and Pd–MgF₂-100 indicating 40, 71 (both aqueous), or 100% (alcoholic) HFA, respectively. For comparison, 1 wt% Pd–MgO was synthesized by a similar procedure,

except that Millipore water was added instead of HFA to the mixture of magnesium methoxide solution and methanolic palladium acetate solution with 1 wt% palladium loading, followed by drying at RT then at 250 °C.

Catalyst characterization

Crystallinity and phase purity of the samples were determined using XRD. Powder patterns were recorded on a X'pert Pro PANalytical X-ray diffractometer with Ni-filtered $\text{CuK}\alpha$ radiation (40 kV, 30 mA) in the 2θ range of 10–80° at a scan rate of 4° min⁻¹ on glass substrate. The specific BET surface area of the samples was determined by acquiring adsorption–desorption isotherm (BET method) at 77 K for N₂ gas by using an Autosorb Quanta Chrome corporation instrument. The micropore volume was estimated from the t plot and the pore diameter by using the BJH model. NH₃-TPD measurements were performed on a Micromeritics AutoChem 2910 instrument. In a typical experiment, 0.1 g of catalyst was taken in a U-shaped flow-through quartz sample tube. Prior to measurements, the catalyst was pretreated in He (30 cm³ min⁻¹) at 400 °C for 1 h. A mixture of NH₃ in He (10%) was passed (30 cm³ min⁻¹) at 25 °C for 1 h. Then, the sample was flushed with He (30 cm³ min⁻¹) at 100 °C for 1 h. The TPD measurements were performed in the range 100–800 °C at a heating rate of 10 K min⁻¹. Ammonia concentration in the effluent was monitored with a gold-plated, filament thermal conductivity detector (TCD). The amount of desorbed ammonia was determined based on the area under the peak. Hydrogen temperature-programmed reduction experiments were carried on a Micromeritics AutoChem 2910 instrument: 0.1 g of the catalyst was placed in a quartz tube and treated with an O₂/He 22:78 (v/v) gas mixture (30 cm³ min⁻¹) at 250 °C for 2 h. A H₂/Ar 5:95 (v/v) gas mixture was then passed (50 cm³ min⁻¹) through the quartz reactor at 50 °C for 1 h. The temperature was raised to 300 °C at a heating rate of 10 K min⁻¹ and held at 300 °C for 0.5 h. The amount of hydrogen consumed was estimated and the reduction capacity of the catalyst determined. A standard CuO powder was used to calibrate the level of H₂ consumption. The elemental composition on the catalyst surface and catalyst morphology were determined by EDX analysis coupled with FEI Quanta 200 3D SEM by using an Al sample holder on C film. Pd particle size was determined by TEM measurements on a Tecnai F20 instrument operated at an accelerating voltage of 200 kV. The TEM grids were prepared by dispersing the powder in 2-propanol by using ultrasound. The suspension was dropped by micropipette on a conventional C film with a thickness of approximately 20 nm supported by a Cu grid. After complete evaporation of 2-propanol from the specimen, the TEM imaging was performed. XPS was performed by using a VG Micro Tech ESCA 3000 instrument at a pressure below 0.13 μPa. The samples were mounted on sample tubs. The wide scan C1s, O1s, F1s, Pd3d and Mg2p core-level spectra were recorded with monochromatic AlK_α radiation ($h\nu = 1486.6$ eV) at a pass energy of 50 eV and electron take-off angle of 60°. The core-level binding energies were aligned by taking an “adventitious” carbon binding energy of 284.6 eV. All peaks were fitted with Gauss–Lorentz peaks by using XPSPEAK41 software to obtain peak information. A Shirley's base line was used in the fitting process. A Nicolet Nexus 670 FTIR instrument with a deuterated triglycine sulfate detector was used to record the IR spectrum of the catalyst in the 4000–400 cm⁻¹ range with the KBr pallet technique in transmission mode. In situ FTIR analysis was performed by using a diffuse-reflectance FTIR accessory in a Shimadzu FTIR 8300 spectrometer equipped with a HgCdTe cryodetector. Data were collect-

ed in the 700–4000 cm⁻¹ range at 4 cm⁻¹ resolution over 100 scans.

Procedure for catalytic hydrogenation reaction

CAUTION: During bubbling H₂ is liberated, therefore all reactions must be performed in a fume hood with high safety measures.

A two-necked round-bottom flask (25 mL) was charged with substrate (5.0 mmol), toluene (6 mL) and catalyst (10 wt% with respect to substrate). The reaction mixture was stirred at 1200 rpm at RT and H₂ gas was bubbled through the reaction mixture at a flow of 10 mL min⁻¹. The reaction was monitored by gas chromatographic analysis by using an Agilent 6890 gas chromatograph equipped with a HP-5 dimethyl polysiloxane capillary column (60 m length, 0.25 mm internal diameter, 0.25 μm film thickness) with a flame ionization detector. Products were confirmed by comparison with spectra of authentic samples.

Acknowledgements

V.R.A. acknowledges the University Grant Commission, New Delhi, India for a research fellowship and Dr. N. Lingaiah, Principal Scientist, CSIR-IICT, Hyderabad, India for hydrogen chemisorption studies. Financial support by CSIR India and BMBF Germany is acknowledged for the Indo–German collaborative project.

Keywords: alkenes · heterogeneous catalysis · hydrogenation · magnesium fluorides · palladium

- [1] a) R. Si, M. F. Stephanopoulos, *Angew. Chem. Int. Ed.* **2008**, *47*, 2884–2887; *Angew. Chem.* **2008**, *120*, 2926–2929; b) L. J. Liu, Z. J. Yao, Y. Deng, F. Gao, B. Liu, L. Dong, *ChemCatChem* **2011**, *3*, 978–989; c) J. F. Liu, W. Chen, X. W. Liu, K. B. Zhou, Y. D. Li, *Nano Res.* **2008**, *1*, 46–55.
- [2] J. M. Campelo, D. Luna, R. Luque, J. M. Marinas, A. A. Romero, *ChemSusChem* **2009**, *2*, 18–45.
- [3] E. Garcia-Bordeje, M. F. R. Pereira, M. Ronning, D. Chenc, *SPR Catal.* **2014**, *26*, 72–108.
- [4] R. Ciriminna, A. Fidalgo, V. Pandarus, F. Beland, L. M. Ilharco, M. Pagliaro, *Chem. Rev.* **2013**, *113*, 6592–6620.
- [5] E. Merino, E. Verde-Sesto, E. M. Maya, M. Iglesias, F. Sanchez, A. Corma, *Chem. Mater.* **2013**, *25*, 981–988.
- [6] Q. M. Kainz, O. Reiser, *Acc. Chem. Res.* **2014**, *47*, 667–677.
- [7] a) X. Y. Liu, M. H. Liu, Y. C. Luo, C. Y. Mou, S. D. Lin, H. K. Cheng, J. M. Chen, J. F. Lee, T. S. Lin, *J. Am. Chem. Soc.* **2012**, *134*, 10251–10258; b) K. Bramhaiah, N. S. John, *RSC Adv.* **2013**, *3*, 7765–7773.
- [8] a) S. J. Tauster, S. C. Fung, R. L. Garten, *J. Am. Chem. Soc.* **1978**, *100*, 170–175; b) Z. H. Qin, M. Lewandowski, Y. N. Sun, S. Shaikhtudinov, H. J. Freund, *J. Phys. Chem. C* **2008**, *112*, 10209–10213.
- [9] a) J. Li, J. L. Chen, W. Song, J. L. Liu, W. J. Shen, *Appl. Catal. A* **2008**, *334*, 321–329; b) Q. Shen, L. Li, C. He, X. Zhang, Z. Hao, Z. Xu, *Asia-Pac. J. Chem. Eng.* **2012**, *7*, 502–509; c) A. S. Ivanova, E. M. Slavinskaya, R. V. Gulyaev, V. I. Zaikovskii, O. A. Stonkus, I. G. Danilova, L. M. Plyasova, I. A. Polukhina, A. I. Boronin, *Appl. Catal. B* **2010**, *97*, 57–71.
- [10] a) Y. Li, W. Shen, *Chem. Soc. Rev.* **2014**, *43*, 1543–1574; b) X. Yao, F. Gao, *Chin. J. Catal.* **2013**, *34*, 1975–1985.
- [11] a) Z. Ma, F. Zaera, *Design of Heterogeneous Catalysis: New Approaches Based on Synthesis Characterization, and Modelling* (Ed.: U. S. Ozkan), Wiley-VCH, Weinheim, **2009**, pp. 113–140.
- [12] a) S. Wuttke, S. M. Coman, G. Scholz, H. Kirmse, A. Vimont, M. Daturi, S. L. M. Schroeder, E. Kemnitz, *Chem. Eur. J.* **2008**, *14*, 11488–11499; b) E. Kemnitz, U. Gross, S. Rüdiger, S. Shekar, *Angew. Chem. Int. Ed.* **2003**, *42*, 4251–4254; *Angew. Chem.* **2003**, *115*, 4383–4386.
- [13] S. M. Coman, S. Wuttke, A. Vimont, M. Daturi, E. Kemnitz, *Adv. Synth. Catal.* **2008**, *350*, 2517–2524.

- [14] P. T. Patil, A. Dimitrov, J. Radnik, E. Kemnitz, *J. Mater. Chem.* **2008**, *18*, 1632–1635.
- [15] A. Negoii, S. Wuttke, E. Kemnitz, D. Macovei, V. I. Parvulescu, C. M. Teodorescu, S. Coman, *Angew. Chem. Int. Ed.* **2010**, *49*, 8134–8138; *Angew. Chem.* **2010**, *122*, 8311–8315.
- [16] N. Candu, S. Wuttke, E. Kemnitz, S. M. Coman, V. I. Parvulescu, *Appl. Catal. A* **2011**, *391*, 169–174.
- [17] S. M. Coman, V. I. Parvulescu, S. Wuttke, E. Kemnitz, *ChemCatChem* **2010**, *2*, 92–97.
- [18] I. K. Murwani, K. Scheurell, E. Kemnitz, *Catal. Commun.* **2008**, *10*, 227–231.
- [19] K. Teinz, S. Wuttke, F. Börno, J. Eicher, E. Kemnitz, *J. Catal.* **2011**, *282*, 175–182.
- [20] H. G. Prechtel, M. Teltewskoi, A. Dimitrov, E. Kemnitz, T. Braun, *Chem. Eur. J.* **2011**, *17*, 14385–14388.
- [21] S. B. Troncea, S. Wuttke, E. Kemnitz, S. M. Coman, V. I. Parvulescu, *Appl. Catal. B* **2011**, *107*, 260–267.
- [22] T. W. Lyons, M. S. Sanford, *Chem. Rev.* **2010**, *110*, 1147–1169.
- [23] J. F. Hartwig, *Organotransition metal chemistry from bonding to catalysis*, University Science Books, **2010**.
- [24] P. W. N. M. van Leeuwen, *Homogeneous catalysis, understanding the art*, Kluwer Academic Publishers, **2004**.
- [25] M. J. Climent, A. Corma, S. Iborra, *Chem. Rev.* **2011**, *111*, 1072–1133.
- [26] J. Tsuji, *Palladium reagents and catalysts, new perspectives for the 21st century*, Wiley, **2004**.
- [27] D. Astruc, *Nanoparticles and catalysis*, Wiley-VCH, **2008**.
- [28] A. Binder, M. Seipenbusch, M. Muhler, G. Kasper, *J. Catal.* **2009**, *268*, 150–155.
- [29] J. Dupont, G. S. Fonseca, A. P. Umpierre, P. F. P. Fichtner, S. R. Teixeira, *J. Am. Chem. Soc.* **2002**, *124*, 4228–4229.
- [30] M. Dell'Anna, M. Gagliardi, P. Mastrorilli, G. P. Suranna, C. F. Nobile, *J. Mol. Catal. A* **2000**, *158*, 515–520.
- [31] R. Andrés, E. de Jesus, J. C. Flores, *New J. Chem.* **2007**, *31*, 1161–1191.
- [32] R. S. Oosthuizen, V. O. Nyamori, *Platinum Met. Rev.* **2011**, *55*, 154–169.
- [33] a) S. Nishimura, *Handbook of Heterogeneous Catalytic Hydrogenation for Organic Synthesis*, Wiley, New York, **2001**; b) P. N. Rylander, *Hydrogenation Methods*, Academic Press, New York, **1985**.
- [34] a) R. Narayanan, M. A. El-Sayed, *J. Am. Chem. Soc.* **2003**, *125*, 8340–8347; b) S. W. Kim, M. Kim, W. Y. Lee, T. Hyeon, *J. Am. Chem. Soc.* **2002**, *124*, 7642–7643.
- [35] M. H. Tran, H. Okhita, T. Mizushima, N. Kakuta, *Appl. Catal. A* **2005**, *287*, 129–134.
- [36] E. Kemnitz, S. Wuttke, S. M. Coman, *Eur. J. Inorg. Chem.* **2011**, 4773–4794.
- [37] a) Y. Diao, W. Walawender, C. S. Sorensen, K. J. Klabunde, T. Ricker, *Chem. Mater.* **2002**, *14*, 362–368; b) K. T. Ranjit, K. J. Klabunde, *Chem. Mater.* **2005**, *17*, 65–73; c) L. Andrews, X. U. Wang, M. E. Likhani, L. Manceron, *J. Phys. Chem. A* **2001**, *105*, 3052–3063.
- [38] M. Zieliński, M. Pietrowski, M. Wojciechowska, *Pol. J. Environ. Stud.* **2009**, *18*, 965–969.
- [39] S. Wuttke, C. Dietel, F. M. Hinterholinger, H. Hintz, H. Langhals, T. Bein, *J. Phys. Chem. C* **2010**, *114*, 5113.
- [40] H. A. Prescott, Z. J. Li, E. Kemnitz, J. Deutsch, H. J. Lieske, *Mater. Chem.* **2005**, *15*, 4616–4628.
- [41] S. Wuttke, S. M. Coman, G. Scholz, H. Kirmse, A. Vimont, M. Daturi, S. L. M. Schroeder, E. Kemnitz, *Chem. Eur. J.* **2008**, *14*, 11488–11499.
- [42] M. Fadoni, L. Lucarelli, *Stud. Surf. Sci. Catal.* **1999**, *120A*, 177–225.
- [43] K. V. R. Chary, D. Naresh, V. Vishwanathan, M. Sadakane, W. Ueda, *Catal. Commun.* **2007**, *8*, 471–477.
- [44] V. I. Nefedov, Y. V. Salyn, I. I. Moiseev, A. P. Sadovskii, A. S. Berenbljum, A. G. Knizhnik, S. L. Mund, *Inorg. Chim. Acta* **1979**, *35*, L343–L344.
- [45] D. D. Eley, H. Pines, *Advances in Catalysis*, Academic Press Inc., US, **1993**.
- [46] B. M. Choudary, S. Madhi, N. S. Chowdari, M. L. Kantam, B. Sreedhar, *J. Am. Chem. Soc.* **2002**, *124*, 14127–14136.
- [47] a) L. Rasmussen, C. K. Jorgensen, *Acta Chem. Scand.* **1968**, *22*, 2313–2323; b) Z. Zhang, W. M. H. Sachtler, H. Chen, *Zeolite* **1990**, *10*, 784–789; c) K. I. Shimizu, R. Maruyama, S. I. Komai, T. Kodama, K. Y. Kitayama, *J. Catal.* **2004**, *227*, 202–209.
- [48] J. Noack, F. Emmerling, H. Kirmse, E. Kemnitz, *J. Mater. Chem.* **2011**, *21*, 15015–15021.
- [49] M. L. Kantam, R. Kishore, J. Yadav, M. Sudhakar, A. Venugopala, *Adv. Synth. Catal.* **2012**, *354*, 663–669.
- [50] A. V. Biradar, A. A. Biradar, T. Asefa, *Langmuir* **2011**, *27*, 14408–14418.
- [51] a) M. Zieliński, M. Wojciechowska, *Catal. Commun.* **2012**, *18*, 1–4; b) M. Zieliński, M. Pietrowski, M. Wojciechowska, *ChemCatChem* **2011**, *3*, 1653–1658; c) M. Zieliński, M. Wojciechowska, *Catal. Today* **2011**, *169*, 175–180.
- [52] B. S. Furniss, A. J. Hannaford, P. W. G. Smith, A. R. Tatchell, *Vogel's Textbook of Practical Organic Chemistry, 5th ed.*, Longman Scientific & Technical, **1989**.

Received: June 24, 2014

Revised: July 10, 2014

Published online on September 11, 2014